HIGHLY INTEGRATED, RADIATION-HARDENED, MOTOR CONTROLLER WITH PHASE CURRENT MEASUREMENT

M. Maier*, J. Reill, H.-J. Sedlmayr, and M. Chalon

DLR (German Aerospace Center), Institute of Robotics and Mechatronics, Muenchner Str. 20, 82234 Wessling, Germany
*E-mail: *Maximilian.Maier@dlr.de*

ABSTRACT

Robotic systems provide an excellent on-site or remote support for astronauts during routine tasks and perform increasingly complex autonomous tasks during exploration missions. The dexterity and the performance of the robotic systems is increasing rapidly, enabling new missions and providing an ever increasing support to the scientific community as well as new business opportunities. The small exploration system MASCOT highlighted the need for a small form factor, highly integrated and high performance motor controller ([1] and [2]). This paper presents a non redundant, three phase brushless DC motor driver for medium radiation environment which was developed at the Institute of Robotics and Mechatronics of the German Aerospace Center (DLR-RM).

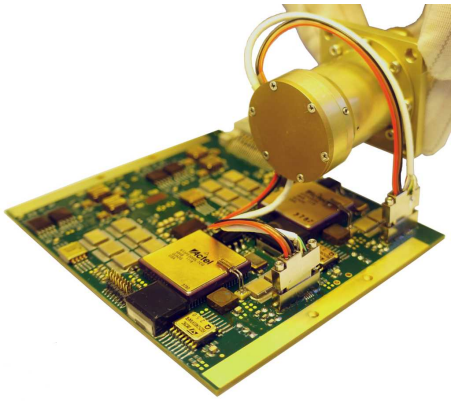

Figure 1. Photo image taken from the mobility flight model showing the PCB and estimated installation position of the motor.

1. INTRODUCTION

Fig. 1 shows the flight model of the MASCOT mobility controller PCB and motor without eccentric arm. This electronics was used as baseline for the development of the controller, since the demand of highly integrated motion control boards is increasing due to the increasing number of robotic exploration systems with arms, pan-tilt units [3] and multiple motor driven mechanisms [4], where the space restrictions are rather strong.

This newly developed, three phase brushless DC motor driver for medium radiation environment offers analogue and digital interfaces for position sensing circuits like resolver or magneto resistive sensors as well as an integrated bridge driver with current limitation, which is able to deliver motor power up to 300 W.

In addition to the sophisticated position sensing interface a three phase current sensing stage is realized, too. This allows the implementation of high level current control like field oriented control methods. These control methods optimize the dynamic performance of the actuator, reduce the power consumption and the system noise of the motor supply stage. The used fault-tolerant processor guarantees a medium range performance and high reliability.

Furthermore the choice of several standard communication interfaces gives the user multiple possibilities to integrate the board in existing designs. The small form factor improves and simplifies the thermal management as well as the integration in small systems.

2. ELECTRONICS

The board is featuring a soft core CPU, power conditioning and distribution modules, customizable sensors and communication interface, as well as an integrated power inverter for a brushless DC motor. The first section describes the overall board architecture and functionality while the subsequent sections give more details about some of the most important technical aspects.

2.1. Architecture

The block diagram in Fig. 2 shows the motor controller which can be used to control motors up to 300 W (from 12 V to 36 V). It offers several communication options such as Spacewire, EtherCAT and RS422. The board provides a three phase current measurement that allows to implement field oriented control methods as well as switch-

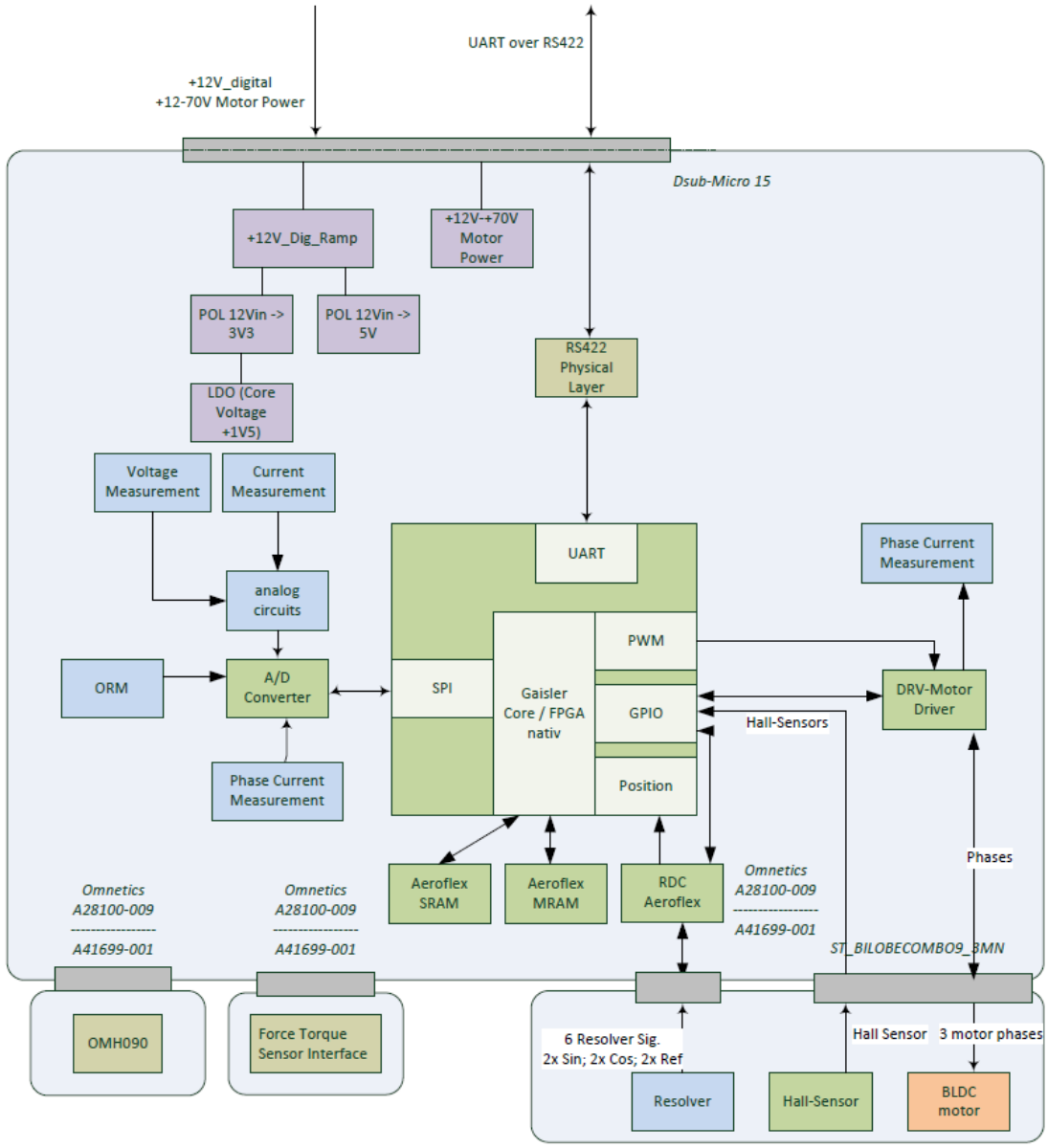

Figure 2. Block diagram

ing mode controllers and more simple commutation patterns. The motor commutation and position feedback can be provided by various sensors, e.g. resolver, hall effect sensors or optical sensors. The FPGA can access a fast SDRAM as well as a non volatile MRAM memory to safe for example calibration data. The board also features several temperature sensors and a radiation monitor. The soft core embedded in the FPGA allows to easily program new functionalities such as logging, automatic check-out procedures or calibration methods.

2.2. Bridge

The power inverter is implemented by the combination of the DRV8332 and the generation of driving signals from the FPGA. In the case of field oriented control the bridges are driven by complementary signals, in the case of a six-steps commutation scheme, a unipolar driving scheme is used. The bridge is providing over-temperature and fault detections. The bridge is primarily intended to drive a three phase brushless motor but can easily be adapted to drive three independent current sinks.

2.3. Soft-core

The motor controller is build around a soft-core CPU implementation in the RT3PE FPGA. Providing very high flexibility, custom specialized functions while guaranteeing a high tolerance to radiation. The non-critical motor control program parts can be written in C programming

language whereas critical code sections, e.g. for the commutation patterns, are implemented directly in the fabric. This architecture ensures the determinism of the motor control loop and remains flexible with respect to the implementation of interfacing code, extra house keeping functions and any non hard realtime task.

2.4. Current measurement

The currents in the motor phases are measured with the help of current sense resistors amplified by the AD8041 and subsequently digitalized by the ADC128S102. Such measurement principle implies that the currents can only be measured when all the lower bridges are conducting to ground. That is, the maximum achievable PWM is lower than 100% to ensure that the time when all the bridges are low is sufficiently long to measure the currents. It is theoretically sufficient to measure two out of the three phases since the sum of the current must be zero. However, measuring three phases allows to improve the measurement accuracy as well as estimate the DC offset of the amplifiers.

The currents of the three phases are sampled simultaneously by three parallel ADCs (ADC128S102). Indeed, because a low side current measurement relies on the decay of the currents in the inductors and suffers a significant error if the three phases are sampled sequentially.

2.5. Resolver

Position sensing for motors is essential to implement energy efficient control algorithm. Unfortunately, many of the well established technologies that are applied in industry are not suitable for space applications. Optical encoders are known to degrade over time, mostly because of the degradation of the optical components. Potentiometers are also suffering surface degradation and need special care when used with high speed motors. Resolvers provide an elegant solution but are often ignored because motor controllers are rarely including an appropriate interface. The RDC5028 from Cobham is a radiation hardened encoder driving and reading chip that survives up to 1MRad. The high resolution, it provides between 10bits and 16bits, at speeds up to 10'000 RPM, makes it ideal for the control of a robotic joint.

2.6. Redundancy

While redundancy might increase the reliability, it comes at the price of an increased complexity and size. Therefore, the design focused on achieving the highest reliability by design and safety margins without sacrificing the valuable space. If a mission requires an even higher reliability, two of the boards can be used in parallel, in the classical cold redundant concept. In such a case, the total area required for the two PCBs does not exceed the area required by an equivalent redundant design, such as the MASCOT mobility controller (cf. Fig. 1). This approach offers a much higher flexibility for system integration, allowing for example any redundancy scheme between full redundant (n+n) to single redundant (n+1). A decoupling network to use more than one electronics with only one motor was introduced in [2].

3. RADIATION PERFORMANCE

Although the motor controller is mostly composed of radiation tolerant parts, some automotive graded parts have been introduced in order to achieve the compact form factor. The approach simultaneously reduce the board size and reduces costs which is in line with the NewSpace philosophy. The use of automotive grade parts is limited to two single parts. An integrated three phase motor driver chip and - if used - the EtherCAT slave controller chip [5].

The use of an EtherCAT slave controller chip is depending on the integration requirements and can be replaced by a fully qualified bus such as Spacewire [6]. Therefore, this paper focuses on the radiation performance of the integrated three phase PWM motor driver chip produced by Texas Instruments, the DRV8332. The radiation tests where performed by the DLR institute at the Helmholtz Zentrum Berlin Wannsee, Germany [7] (TID and protons) and at the radiation effects facility in Jyvaskyla, Finland [8] (Heavy Ions).
The TID irradiation was performed at room temperature with a Co60 source at a dose rate of 4.95 Gy(Si)/h. All relevant parameters were measured in-situ during the irradiation, therefore no pre-irradiation steps was required. This approach requires a longer testing time but allows to identify effects that are sometimes occurring in the low radiation doses. The test consisted of making a BLDC (brushless direct current) motor spin under the control of the motor driver chip commanded by a suitable commutation pattern generated by a FPGA. During the irradiation the motion of the motor was monitored by two independent position measurement systems and synchronized with the parameter measurements. Any malfunction of the driver chip can be identified by a sudden rise of the motor current and/or an interruption of the motor rotation. Although this methodology requires to build and program a motor driving unit, it ensures that the motor driver chip is used in realistic conditions that are hard to emulate with passive loads such as coils and power resistors.
No significant effects were observed up to a total dose of 550 Gy(Si), when the test was stopped. Fig. 3 shows the monitoring of the device temperature (left sub-figure) and the output voltage of the internal reference voltage (right sub-figure), where a minor degradation above 400 Gy(Si) is visible. To increase the clarity of the plot, the measured values were plotted for sub-sample of the measured values.

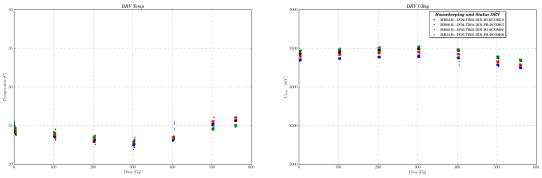

Figure 3. Device temperature and reference voltage output

Fig. 4 shows the supply currents of the digital logic at 12 V DC (left sub-figure) and the motor supply current at 28 V (right sub-figure). A slight increase of the supply current of the digital logic is visible (45 mA up to 65 mA), but the motor current is stable which shows that the gate driver logic is imperious to the irradiation. Similar to the preceding picture only a subset of the data is plotted to increase the clarity.

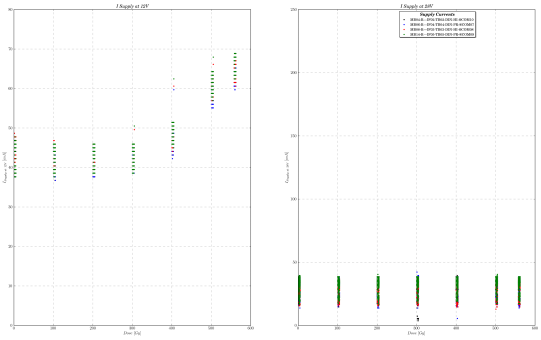

Figure 4. Supply currents during irradiation with Gamma rays

As a second test step, the integrated three phase motor driver chip was irradiated with protons at room temperature. For this test, protons with an energy of 30, 50 and 60 MeV per nucleon were used and a fluence of $1.7 \cdot 10^{10} \frac{Particles}{cm^2}$ was applied for each proton energy. Similar to the Co60 irradiation all important parameters were measured during the irradiation and a rotating BLDC motor was used as load. Fig. 5 shows the digital output values of both position monitors. On the left side, the reference encoder is shown and on the right side the resolver. A disruption of the driver functionality would lead to a motor standing still or an erratic motion of the motor. Similar to the TID test, no significant effect could be observed.

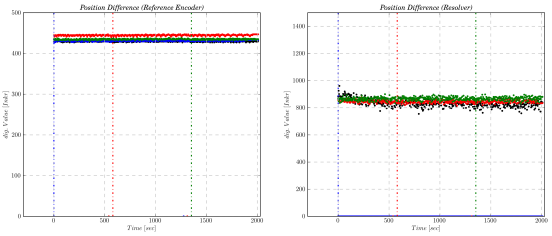

Figure 5. Position difference of motor during proton irradiation

Finally irradiations with high energy ions were performed to conclude the characterization of the radiation performance of the three phase PWM motor driver chip. For this test campaign Ne, Ar, Fe, Kr and Xe ions were used and a fluence of $1.0 \cdot 10^7 \frac{Ions}{cm^2}$ was applied for each ion species. To vary the effective LET (Linear Energy Transfer), several tilt angles were applied.
For this irradiation the package of the three phase driver chip was opened and the irradiation was performed at room temperature in vacuum. Since the package contains an elementary heat sink for this chip, a test with elevated temperature was skipped in order to avoid effects which relays mainly on temperature instead of the applied radiation. Of course, all important parameter were measured during the irradiation and the rotating BLDC motor was used to verify the operation of the chip, too.
Up till an effective LET of $LET_{max} = 55.6 \frac{MeV \cdot cm^2}{mg}$ no significant effect was observed. When irradiating with Xe ions which corresponds to an effective LET of $LET_{th} = 59.9 \frac{MeV \cdot cm^2}{mg}$ the three phase motor controller stopped its operation. But no catastrophic event like Latch-up or shot-through could be measured at this state of operation for both supply voltages.
When analyzing the measured values more in detail, a slightly raised temperature in conjunction with a slightly increased supply current was recorded which points toward a micro-Latch-up in the control area of the chip. But the existing shot-through protection as well as the short-circuit detection for the load of the driver chip prevents the chip from running into a critical operational state.
Since the three phase PWM motor driver chip is the critical part on the motor driver board, the radiation limits of the motor driver board shall be set to a total ionizing dose of 500 Gy(Si) and for particle radiation to a LET of $LET_{max} = 55.6 \frac{MeV \cdot cm^2}{mg}$.

4. MOTOR CONTROL STRATEGIES

As the developed electronics was designed to drive a permanent magnet synchronous motor (also named as brushless DC-motor BLDC depending on control strategy) it still offers different possibilities to implement the motor controller. From the well known six-step commutation to the advanced field oriented control FOC algorithm even position sensorless control in different complexity level

is feasible. This chapter shows why the authors focus on BLDC motors, gives a brief overview of the different approaches and finally adresses the main advantages and drawbacks of every algorithm.

4.1. Advantages of a BLDC Motor

In space applications it is still very common to use DC-motors. In industry the three phase motors have taken over in almost every discipline. This is due to the general advantages of BLDC motors compared to DC-motors.

- High torque output per volume and weight
- Extreme durability and reliability (higher peak torques)
- Reduced probability of failures because of only very few mechanical parts (no brushes: No brush sparking, no cold welding of brushes and motor collector, no brush wear debris that shortens motor windings and destroys the drive train)
- Much better heat dissipation because the copper windings are located in the stator only

The drawback of BLDC motors is that power electronics needs six MOSFETs compared to only four when using DC-motors. Additionally the motor control algorithm must know the rotor position to spin the motor. It does not move when voltage is applied as it is with DC-motors. Even though this might give the impression of a disadvantage this characteristic can also be treated as an advantage. In almost every space application the mechatronics faces extreme temperatures. This is why a lot of motors have heaters attached. With appropriate control strategies the algorithm is able to split the electric energy drawn into heating and torque generating. It is even possible to use the motor for heating the mechanics only without moving.

4.2. Motor Control Theory

The mathematics used with BLDC motors is based on coordinate transformation and only a few differential equations. The three phases of the motor windings (U, V and W) are described as voltage drop on ohmic resistor and voltage due to current change on inductance. The third portion is induced voltage due to permanent magnets that are moving in front of the winings. This considerations lead to Eq. (1).

$$\underbrace{\begin{pmatrix} u_u \\ u_v \\ u_w \end{pmatrix}}_{\underline{u}_{uvw}} = \underbrace{\begin{pmatrix} R_u & 0 & 0 \\ 0 & R_v & 0 \\ 0 & 0 & R_w \end{pmatrix}}_{\underline{\mathbf{R}}} \cdot \underbrace{\begin{pmatrix} i_u \\ i_v \\ i_w \end{pmatrix}}_{\underline{i}_{uvw}} + + \frac{d}{dt} \left[\underbrace{\begin{pmatrix} L_{uu} & L_{uv} & L_{uw} \\ L_{vu} & L_{vv} & L_{vw} \\ L_{wu} & L_{wv} & L_{ww} \end{pmatrix}}_{\underline{\mathbf{L}}} \cdot \underbrace{\begin{pmatrix} i_u \\ i_v \\ i_w \end{pmatrix}}_{\underline{i}_{uvw}} \right] + + \underbrace{\begin{pmatrix} u_{pu} \\ u_{pv} \\ u_{pw} \end{pmatrix}}_{\underline{U}_p} \tag{1}$$

When voltage is applied to the motor windings that are spaticially rotated by 120°, there is a voltage vector generated that points to the positive or negative direction of the according phase. Fig. 6 shows the six steps that are possible and also a voltage vector that is generated by using two different vectors. When using only the six main steps

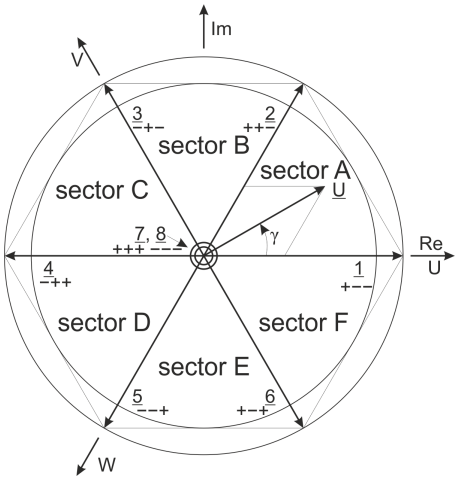

Figure 6. Diagram of voltage vectors given by the motor phases U, V and W that are 120° rotated.

for generating voltage vector in the motor, the control algorithm is usually called six-step commutation. The voltage vector is moving in discrete steps and the rotor position only needs to be measured in low resolution. The algorithm just needs to know the sector and can apply the next voltage vector by use of a simple lookup table. The performance of motor movement is pretty poor considering torque ripple. Still the motor can be used in applications where position and speed need to be controlled only. When it comes to robotic applications and to realize smooth movement trajectories of robotic joints this behavior is not sufficient.

This is when field oriented control needs to be implemented. A more complex algorithm needs to be used and the hardware needs to get a position sensor with higher

resolution. By using the so called Park and Clark transformations the three phases can be mathematically treated as two phases α and β that are bound to the stator windings. In the final transformation this two axis system is rotated by the rotor position and the complex Eq. (1) turns into Eq. (2). The coordinate axes are usually called d- and q-axis. Fig. 7 shows the steps that lead to d and q.

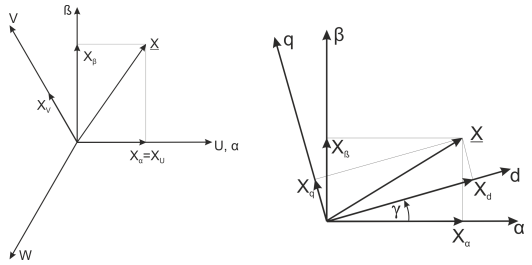

Figure 7. Diagram to illustrate the used coordinate transformations.

$$\begin{aligned} u_d &= R \cdot i_d + L_d \cdot \frac{di_d}{dt} - \omega \cdot L_q \cdot i_q \\ u_q &= R \cdot i_q + L_q \cdot \frac{di_q}{dt} + \omega \cdot L_d \cdot i_d + \omega \cdot \psi_p \end{aligned} \tag{2}$$

Now the motor behavior is described by two coupled differential equations. The q-current directly affects the torque and the d-current should be controlled to zero in a first approach. A torque controller block diagram is given in Fig. 8. For each axis a PI-controller can be used. The

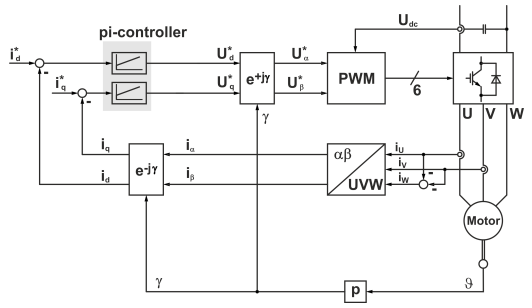

Figure 8. Block diagram of the dq-controller structure used in field oriented control algorithm.

PWM block needs to be used for generating switching signals to the MOSFETs. There exist different strategies to generate these signals. The idea of all algorithms is to mix different voltage vectors within a certain time intervall to get a resulting voltage vector that is located in between the main directions. This way the permanent magnets on the rotor are pulled in a continuous way instead of the discrete six-step pulling that results in torque hopping.

4.3. Position Sensorless Control

The previous subchapter described why the rotor position sensor is mandatory for BLDC motor control. Even when no position or speed control loop is needed in the application there is still the need for a position measurement to ensure correct direction of generated voltage vector. In industry applications the position sensor turned out to be a single point of failure and it also increases cost, weight and volume of the drive system. Therefore in recent years advanced algorithms got proposed that are able to approximate the position signal from motor currents only. In general every sensor increases system knowledge and enables the control algorithm to increase bandwidth and stiffness. If no cutting edge dynamics is needed the sensor is actually replaced by computation power. The authors propose the industry approach to be transferred to space applications. The virtual sensor could detect a hardware sensor failure and increase system reliability. Even when the position sensor gets broken the system is able to keep on driving (maybe at reduced dynamics).

With the proposed electronics two strategies are actually under investigation.

4.3.1. EMF based Algorithm

When the motor is moving the rotor magnets are constantly moving in front of the stator windings. This is causing induced voltages (so called ElectroMtotiveForce) that may be used for position sensorless control. Considering the α-β equations (3) of the motor model the position approximation shown in Fig. 9 gives a first approach on position sensorless control.

$$\begin{aligned} u_\alpha &= R_1 \cdot i_\alpha + L_1 \cdot \frac{di_\alpha}{dt} + \frac{d\psi_\alpha}{dt} \\ u_\beta &= R_1 \cdot i_\beta + L_1 \cdot \frac{di_\beta}{dt} + \frac{d\psi_\beta}{dt} \end{aligned} \tag{3}$$

In [9] this idea is used in a more elaborated way. The

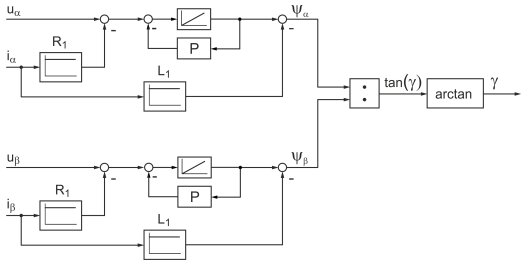

Figure 9. Block diagram showing the principal idea of sensorless control at higher speeds.

constraints that limit this approach is the fact that at low speed and especially at standstill the magnets are not moving and therefore the signal that gives the needed information gets lost. The next subchapter shows an algorithm that is able to overcome this barrier.

4.3.2. HF-Signal based Algorithm

Fig. 10 shows a block diagram that gives a brief overview of the high frequency injection method. Since the induced voltages are of too low amplitude a sinusoidal wave is added to the d-axis voltage. This causes only very little torque ripple since in d-axis the flux of the machine is influenced only. To prevent the current PI-controllers from fighting against that additional current response the motor phase currents need to be filtered. This way the controllers do not get the current response of the voltage modulation. Since filtering is always causing phase lag in the signal it was shown in [10] that the goertzel algorithm offers a perfect way to separate the fundamental wave from the high frequency signal. The frequency that was applied is well known and therefore no complete frequency spectrum needs to be computed. This saves computational effort at no performance cost. The high frequency portion is used in an approximation block to compute the angle of the dq-reference frame that equals the electrical rotor position. If a machine with only one pole pair is used, then electrical and mechanical rotor position are identical.

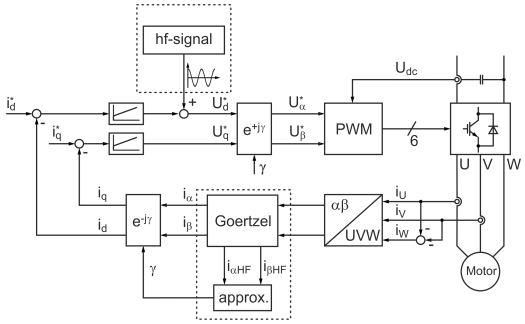

Figure 10. Block diagram showing the principal idea of sensorless control at low speeds or standstill.

5. CONCLUSION

Considering the demand for motion controller hard and software in space applications a compact electronics board was introduced that is very flexible to interfacing needs. Also a way of using a position sensorless algorithm was proposed to make use of a virtual sensor that might replace the sensor completely or serve as a redundancy. All algorithms are under close investigation but also conventional control strategies might be used when integrating the proposed motion controller board. First measurement results look encouraging and this work is continued.

REFERENCES

[1] T.-H. Ho, V. Baturkin, R. Findlay, C. Grimm, J.-T. Grundmann, C. Hobbie, E. Ksenik, C. Lange, K. Sasaki, M. Schlotterer, M. Talapina, N. Termtanasombat, E. Wejmo, L. Witte, M. Wrasmann, G. Wübbels, C. Rößler, J.and Ziach, J. Biele, C. Krause, S. Ulamec, M. Lange, O. Mierheim, J. Lichtenheldt, M. Maier, J. Reill, H.-J. Sedlmayr, P. Bousquet, A. Bellion, O. Bompis, C. Cenac-Morthe, M. Deleuze, S. Fredon, E. Jurado, E. Canalias, R. Jaumann, J.-P. Bibring, K. H. Glaßmeier, M. Grott, L. Celotti, F. Cordero, J. Hendrikse, and T. Okada. MASCOT - The Mobile Asteroid Surface Scout onboard the HAYABUSA2 Mission. In *Space Science Reviews, Volume 1 / 1962 - Volume 199 / 2016*, Springer, April 2016.

[2] J. Reill, H.-J. Sedlmayr, P. Neugebauer, M. Maier, E. Krämer, and E. Lichtenheldt. MASCOT - Asteroid Lander with innovative Mobility Mechanism. In *13th Symposium on Advanced Space Technologies in Robotics and Automation (ASTRA)*, ESA/ESTEC, Noordwijk, Netherlands, May 2015.

[3] A. Wedler, A. Maier, J. Reill, C. Brand, H. Hirschmüller, M. Suppa, A. Beyer, and R. Haarmann. Pan/Tilt-Unit as a perception module for extra-terrestrial vehicle and landing systems. In *12th Symposium on Advanced Space Technologies in Robotics and Automation (ASTRA)*, ESA/ESTEC, Noordwijk, Netherlands, May 2013.

[4] M. Chalon, M. Maier, A. Bertleff, W.and Beyer, R. Bayer, W. Friedl, P. Neugebauer, T. Obermeier, H.-J. Sedlmayr, N. Seitz, and A. Stemmer. SPACE-HAND: a multi-fingered robotic hand for space. In *13th Symposium on Advanced Space Technologies in Robotics and Automation (ASTRA)*, ESA/ESTEC, Noordwijk, Netherlands, May 2015.

[5] EtherCAT. Technology group. $https://www.ethercat.org/$, 2017.

[6] ESA. Spacewire. $https://www.ethercat.org/$, 2017.

[7] Helmholtz Zentrum Berlin Wannsee. Cobalt-60 source. $http://www.helmholtz-berlin.de/angebote/tt-industrie/methoden/kobalt/index_de.html$, 2017.

[8] University of Jyvaskyla. Radiation effects facility - RADEF. $https://www.jyu.fi/fysiikka/en/research/accelerator/radef/facility$, 2017.

[9] S. M. A. Sharkh and V. Barinberg. Design and performance of a new technique for sensorless control of a downhole brushless pm motor. *Power Electronics and Variable Speed Drives*, pages 263–268, September 1998.

[10] J. Reill, B. Piepenbreier, and I. Hahn. Utilisation of magnetic saliency for sensorless-control of permanent-magnet synchronous motors. In *International Symposium on Power Electronics, Electrical Drives, Automation and Motion (SPEEDAM)*, June 2010.